IEEE Access
Multidisciplinary | Rapid Review | Open Access Journal

Received February 11, 2020, accepted March 8, 2020, date of publication March 18, 2020, date of current version March 30, 2020.

Digital Object Identifier 10.1109/ACCESS.2020.2981631

Proactive Uplink Interference Management for Nonuniform Heterogeneous Cellular Networks

MUHAMMAD SAJID HAROON[1], FAZAL MUHAMMAD[2], ZIAUL HAQ ABBAS[3], GHULAM ABBAS[4], (Senior Member, IEEE), NISAR AHMED[3], AND SUNGHWAN KIM[5]

[1]Telecommunications and Networking (TeleCoN) Research Lab, GIK Institute of Engineering Sciences and Technology, Topi 23640, Pakistan
[2]Department of Electrical Engineering, City University of Science and Information Technology, Peshawar 2500, Pakistan
[3]Faculty of Electrical Engineering, GIK Institute of Engineering Sciences and Technology, Topi 23640, Pakistan
[4]Faculty of Computer Science and Engineering, GIK Institute of Engineering Sciences and Technology, Topi 23640, Pakistan
[5]School of Electrical Engineering, University of Ulsan, Ulsan 44610, South Korea

Corresponding author: Sunghwan Kim (sungkim@ulsan.ac.kr)

This work was supported by the Research Program through the National Research Foundation of Korea under Grant NRF-2019R1A2C1005920.

ABSTRACT In homogeneous cellular networks, fractional power control (FPC) is employed to partially compensate the path-loss and, hence, improve uplink (U_L) signal-to-interference ratio (SIR). However, this scheme is less effective in heterogeneous cellular networks (HetNets) because: (i) except the typical user, all other users with variable U_L transmit power (UTP) act as interferers, (ii) FPC leads to high UTP by edge users and, hence, more interference, and (iii) small base stations (SBSs)' densification further increases network interferences. Leveraging FPC in HetNets, we propose nonuniform SBS deployment (NU-SBS$_{\mathcal{D}}$) to reduce interference and, thus, increase network performance. According to our NU-SBS$_{\mathcal{D}}$ model, SBS deployment (SBS$_{\mathcal{D}}$) near macro base station (MBS) is avoided, whereas MBS coverage edge area is enriched with ultra-dense SBS$_{\mathcal{D}}$. NU-SBS$_{\mathcal{D}}$ model leads to: (i) better SIR reception of MBS coverage edge users, (ii) fewer SBS$_{\mathcal{D}}$ requirement, and (iii) better SBS coverage in the MBS coverage edge area. Moreover, to make a model more proactive, we also consider reverse frequency allocation (RFA) to further abate both U_L and downlink (D_L) interferences. The coverage probability expressions are derived for both uniform SBS deployment (U-SBS$_{\mathcal{D}}$) and NU-SBS$_{\mathcal{D}}$ while using RFA and FPC. Through simulation and numerical results, we characterize coverage probability for different values of SIR threshold, path loss compensation factor, SBS density, users density, and the distance between the typical user and the associated base station. The proposed NU-SBS$_{\mathcal{D}}$ model along with RFA leads to reduced network interference as compared with U-SBS$_{\mathcal{D}}$ and, thus, leverages FPC in HetNets.

INDEX TERMS Coverage probability, fractional power control, heterogeneous cellular networks, Poisson point process, Poisson hole process, reverse frequency allocation, interference management.

I. INTRODUCTION

A. MOTIVATION

In heterogeneous cellular networks (HetNets), coverage probability, spectrum efficiency, and throughput are significantly enhanced by enriching coverage area of macro base station (MBS) with small base station deployment (SBS$_{\mathcal{D}}$) [1], [2]. In HetNets, MBS-associated users (MBS-AUs) and SBS-associated users (SBS-AUs) share the same frequency band and, hence, lead to high throughput. However, this aggressive frequency reuse results in severe inter-cell interference (ICI) and, thus, significantly limits the network performance gain [3], [4]. In downlink (D_L) transmission, for instance, SBSs strongly interfere with MBS-AUs in the proximity of SBS coverage. Similarly, in uplink (U_L) transmission, co-channel interference between SBS and MBS also exits [5], [6]. Moreover, orthogonal multiple access (OMA) consideration leads to limited or no intra-cell interference, however, ICI remains one of the main performance limiting factors in HetNets [7].

In HetNets, U_L power control is employed to leverage path-loss, shadowing, small-scale fading, and near-far problem [8].

The associate editor coordinating the review of this manuscript and approving it for publication was Irfan Ahmed.

U_L transmit power (UTP) of a typical user,[1] ν, is dynamically adjusted by following fractional power control (FPC) [10]. The FPC employment in HetNets leads to partial path-loss compensation and, hence, improves U_L signal-to-interference ratio (SIR) [3], [11]. According to FPC, UTP of ν depends on the distance r between ν and its serving base station (BS) [3]. FPC is more effective in homogeneous cellular networks as compared to HetNets because: (i) all other users with variable UTP act as interferers for ν, (ii) FPC requires high UTP by edge users and hence higher interference, and (iii) SBS densification further increases network interference [3], [12].

In this paper, we propose nonuniform SBS$_\mathcal{D}$ (NU-SBS$_\mathcal{D}$) as opposed to uniform SBS$_\mathcal{D}$ (U-SBS$_\mathcal{D}$) in the MBS coverage area. In NU-SBS$_\mathcal{D}$, SBS$_\mathcal{D}$ near MBS is avoided in order to achieve: (i) better edge users' SIR reception, (ii) lower SBS$_\mathcal{D}$, and (iii) larger SBS coverage in MBS coverage edge area [13], [14]. Due to the aforementioned benefits, the proposed NU-SBS$_\mathcal{D}$ with FPC leads to efficient U_L interference mitigation. We employ NU-SBS$_\mathcal{D}$ through Poisson hole process (PHP). According to PHP, the points (SBSs in our case) near the MBS are removed (see Lemma 1 in Sec. II-A).

Moreover, to effectively mitigate ICI, a proactive interference management scheme is required. Different interference management schemes have been proposed in the state-of-the-art to mitigate D_L and U_L interferences, such as fractional frequency reuse (FFR) [15], cell range expansion (CRE) [16], soft frequency reuse (SFR) [17], and reverse frequency allocation (RFA) [18], [19]. In RFA, U_L and D_L sub-carriers are used by SBS-AUs and MBS-AUs in alternate regions and in reverse fashion. In this paper, we use NU-SBS$_\mathcal{D}$ in conjunction with RFA and FPC to improve U_L coverage performance.

B. RELATED WORK

In [20], the authors use FPC and FFR to mitigate U_L interference in 5G networks. They use FPC mechanism within certain geographical areas. The results demonstrate significant interference reduction and enhanced network performance.

In [21], the authors investigate open loop power control (OLPC)[2] parameters for HetNets. Moreover, they perform mathematical analysis to compute UTP of ν, received power of BS, received signal-to-interference-plus-noise ratio (SINR), and network interference. Furthermore, optimum OLPC parameters are also evaluated.

In [22], the authors propose interference-aware U_L power control while adjusting the OLPC parameter. Their proposed model reduces U_L interference and, thus, increases SBS and MBS capacity by 25.6 %. Furthermore, their results verify that close loop power control supports the received SINR of OLPC to meet the target SINR by compensating the fading effect.

For ease of analysis, the authors in [23] and [24] divide MBS coverage region into two sub-regions, i.e., cell interior region and cell edge region. Regular MBS-AUs in the cell edge region experience low SINR due to their far locations [23]. Moreover, offloaded SBS-AUs in the cell interior region experience severe interference due to close proximity with the MBS [24].

In [25], the authors propose NU-SBS$_\mathcal{D}$ with SFR. They investigate both U-SBS$_\mathcal{D}$ and NU-SBS$_\mathcal{D}$ in the MBS coverage area. They demonstrate the effectiveness of SFR together with NU-SBS$_\mathcal{D}$. Their results show that NU-SBS$_\mathcal{D}$, in conjunction with SFR, outperform other scenarios due to proactive interference mitigation. Furthermore, in [26], the authors propose off-grid NU-SBS$_\mathcal{D}$, where SBSs are powered through renewable energy. They investigate the HetNets' performance by considering MBS as on-grid and SBSs as off-grid. Based on the proposed model, they obtain association probabilities, distance distributions, and coverage probabilities. In [14], the authors investigate D_L coverage while considering non-orthogonal multiple access in HetNets with NU-SBS$_\mathcal{D}$. Moreover, they analyze coverage and energy efficiency of the proposed model. Similarly in [27], RFA along with NU-SBS$_\mathcal{D}$ are considered. The authors assume the SBSs to be muted[3] in the cell interior region and active in the cell edge region. Expressions for both coverage probabilities and rate coverage are derived. Their results indicate that NU-SBS$_\mathcal{D}$ in MBS coverage edge region significantly improves the rate coverage. In [28], a modified RFA is proposed, which leads to improved coverage as opposed to other schemes.

The novelty of this work is as follows.

1) The works in [20]–[22] lack the analysis of FPC with RFA and NU-SBS$_\mathcal{D}$, which is performed in this paper.
2) In [27], NU-SBS$_\mathcal{D}$ is employed by cell muting, however, we employ NU-SBS$_\mathcal{D}$ through PHP.
3) In [14] and [27], D_L coverage analysis are performed, however, in this paper, we perform U_L coverage analyses.
4) The works in [14], [23]–[28] lack the analysis of FPC. This paper analyzes NU-SBS$_\mathcal{D}$ along with RFA and FPC.

C. APPROACH AND CONTRIBUTIONS

In this paper, a two-tier HetNet model is considered, where U-SBS$_\mathcal{D}$ and NU-SBS$_\mathcal{D}$ are assumed, as shown in Fig. 1 (see Sec. II-C for details on U-SBS$_\mathcal{D}$ and NU-SBS$_\mathcal{D}$). The performance of the proposed model is evaluated in a tractable manner by using stochastic geometry framework. The coverage region of MBS is split into two non-intersecting regions, i.e., center region, A^c_{M}, and outer region, A^o_{M}, with radii d_1 and d_2, respectively. Additionally, we employ RFA together with NU-SBS$_\mathcal{D}$ and FPC to abate ICI and, thus, improve network performance.

[1] Following Slivnyak theorem, a typical user at origin leads to simplified statistical properties of an independent homogeneous Poisson point process (IHPPP) [9].

[2] The terms open loop power control and FPC are used interchangeably in this paper.

[3] The muted-SBS region refers to the cell interior region of MBS, wherein the SBSs are muted.

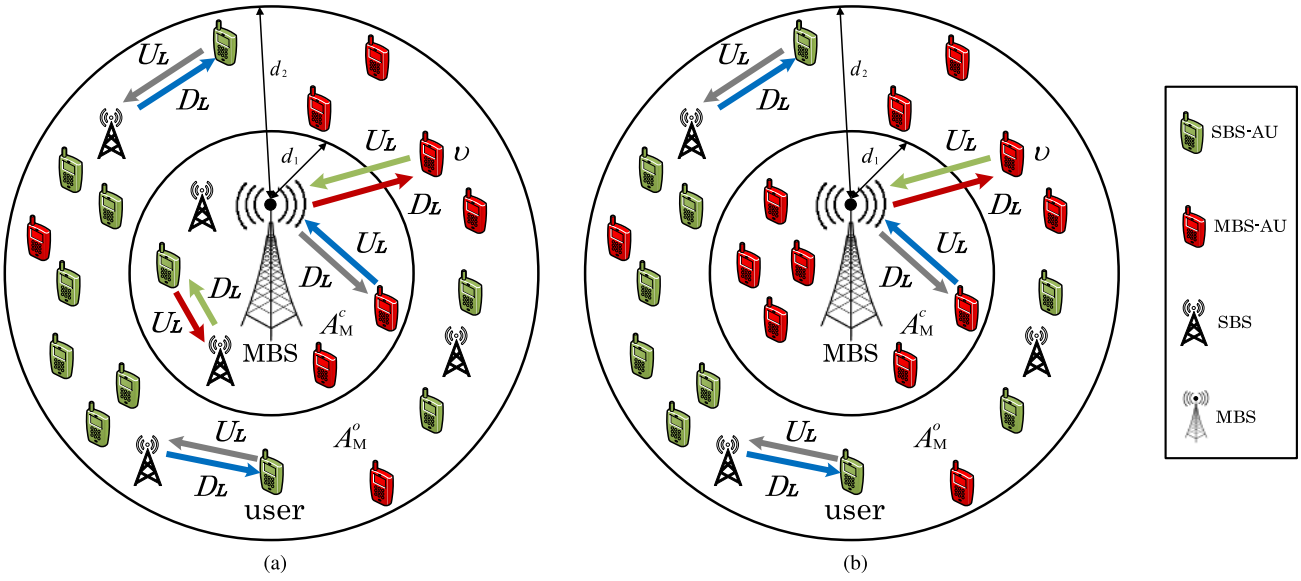

FIGURE 1. A two-tier HetNet model, where ϕ_M, $\phi_{M,\nu}$ and $\phi_{S,\nu}$ are the IHPPPs of MBSs, MBS-AU and SBS-AU, respectively, with (a) indicating U-SBS$_\mathcal{D}$ model and (b) indicating NU-SBS$_\mathcal{D}$ model.

The main contributions of this paper are as follows.

1) We propose an NU-SBS$_\mathcal{D}$ model along with RFA to overcome ICI and, thus, leverage FPC in HetNets. The proposed model leads to improved U_L coverage, as compared with the U-SBS$_\mathcal{D}$ model along with FPC and RFA.
2) We characterize coverage probabilities of the proposed model for different values of the fractional path loss compensation factor, ϵ, i.e., $\epsilon = 0, 0.2, 0.6, 0.8, 1$. Moreover, coverage analysis is performed on ν located in both A_M^c and A_M^o.
3) We use RFA along with the proposed FPC based NU-SBS$_\mathcal{D}$. The RFA employment leads to better ICI mitigation and, thus, makes the FPC more effective.
4) We derive coverage probability expressions for the following scenarios: (i) U-SBS$_\mathcal{D}$ with FPC and RFA (see Sec. III-A1), (ii) U-SBS$_\mathcal{D}$ with FPC and without RFA (see Sec. III-A2), (iii) NU-SBS$_\mathcal{D}$ with FPC and RFA (see Sec. III-B1), and (iv) NU-SBS$_\mathcal{D}$ with FPC and without RFA (see Sec. III-B2).
5) We evaluate coverage probability against ϵ, SIR threshold, densities of MBS-AUs, MBSs and SBSs.
6) The results indicate significant U_L coverage improvement by NU-SBS$_\mathcal{D}$ with FPC and RFA as compared with U-SBS$_\mathcal{D}$ with FPC and RFA.

TABLE 1. Notations.

Notation	Description
ϕ_M, ϕ_S	IHPPPs of MBSs and SBSs, respectively
ν	A typical user
β_ν	SIR threshold for ν
d_1	Radius of A_M^c
$P_{t,\nu}^{U_L}$	U_L transmit power of MBS-AUs
λ_M, λ_S, $\lambda_{M,\nu}$	Densities of MBSs, SBSs, and MBS-AUs, respectively
$\tilde{\lambda}_S$	NU-SBS$_\mathcal{D}$ based SBS density
α	Path loss exponent, $\forall\ \alpha_M = \alpha_S = \alpha$ and $\alpha > 2$
A_M^g, A_S^g	Coverage regions of MBS and SBS, s.t., $g \in \{c, o\}$
$\lvert h\rvert$	Power gain of Rayleigh fading
D_L, U_L	Downlink and uplink
r_j, r_k	User distances from jth- and kth-tiers, $\forall\ j \in \{\phi_M\}$ and $k \in \{\phi_S\}$
$\text{SIR}_\nu^{U_L}$	U_L SIR received by iBS, $\forall\ i \in \{M, S\}$
$r_{M,\nu}$	Distance between MBS and ν
$*$	NU-SBS$_\mathcal{D}$
η_1	Ratio of $P_S^{D_L}$ and $P_{t,\nu}^{U_L}$
ϵ	Fractional path loss compensation factor

D. PAPER ORGANIZATION AND NOTATIONS

The rest of the paper is organized as follows. In Sec. II, we present the system model. In Sec. III, coverage probability expressions are derived for the proposed model. Simulation and numerical results are presented and discussed in Sec. IV. In Sec. V, the paper is concluded. Table 1 lists the notations used in this paper.

II. SYSTEM MODEL

This section focuses on both U-SBS$_\mathcal{D}$ (see Fig. 1a) and NU-SBS$_\mathcal{D}$ (see Fig. 1b) models, with RFA and FPC employments. In the U-SBS$_\mathcal{D}$ model (see Subsec. III-A), MBSs, SBSs, and users are distributed through IHPPPs. However, in NU-SBS$_\mathcal{D}$ (see Subsec. III-B), MBSs and users are distributed using

IHPPPs while SBSs are distributed through PHP, as shown in Fig. 1b.

A. NETWORK LAYOUT WITH ASSUMPTIONS

A two-tier HetNet model, comprising of MBSs and SBSs with densities λ_{M} and λ_{S}, respectively, is considered. In the U-SBS$_{\mathcal{D}}$ model, users, SBSs, and MBSs are distributed using IHPPPs, ϕ_u, ϕ_{S} and ϕ_{M}, respectively. However, in NU-SBS$_{\mathcal{D}}$, users and MBSs are distributed using IHPPPs, ϕ_u and ϕ_{S}, respectively, while SBSs are deployed through PHP, $\tilde{\phi}_{\mathrm{S}}$. A typical user, ν, is considered at the origin by following the Slivnyak's theorem [18]. As interference is the dominant performance limiting factor, therefore, noise is neglected. α_{M} and α_{S} are the path loss exponents for MBS and SBS, respectively, s.t., $\alpha_{\mathrm{M}} = \alpha_{\mathrm{S}} = \alpha$, due to the outdoor model consideration. $|h|$ denotes Rayleigh fading gain. Users are associated with a BS through maximum long term average received power strategy [29]. d_1 is the radius of A^c_{M} while d_2 is the radius of A^o_{M} around MBS [30]. Definition 1 defines PHP, while Lemma 1 defines the effective SBS density, $\tilde{\lambda}$, under NU-SBS$_{\mathcal{D}}$ assumption.

Definition 1: (Poisson hole process) Let ϕ_1 and ϕ_2 be two IHPPPs with intensities λ_1 and λ_2, respectively. Further, let

$$\Xi \triangleq \bigcup \{x \in \phi_1 : b(x, r)\} \tag{1}$$

be the union of all disks of radius r centered at a point of ϕ_1. The PHP is defined as

$$\phi \triangleq \phi_2 \backslash \Xi. \tag{2}$$

In the PHP, each point in ϕ_1 carves out a hole of radius r from ϕ_2 [9].

Lemma 1: In NU-SBS$_{\mathcal{D}}$ through PHP, the effective SBS density, $\tilde{\lambda}$, is given as

$$\tilde{\lambda}_S = p\lambda_S = \lambda_S exp(-\lambda_M \pi d_1^2). \tag{3}$$

Proof: By following PHP, we consider radius of exclusion area, d_1, around MBS, i.e., A^c_{M}. Moreover, for each point $j \in \phi_{\mathrm{M}}$, all the points of $\phi_{\mathrm{S}} \bigcap A^c_{\mathrm{M}}(j, d_1)$ are removed. Hence, the effective density of SBSs in the proposed model is given as $p\lambda_{\mathrm{S}}$, where $p = \exp(-\lambda_{\mathrm{M}} \pi d_1^2)$ [30]. ■

B. FPC MECHANISM

In this paper, we consider both large scale and small scale fadings. For large scale fading, we assume standard path loss model while for small scale fading, Rayleigh fading model is assumed. D_L transmit power for iBS $\forall\ i \in$ (M,S) is fixed while UTP follows FPC. According to FPC, UTP of ν is dynamically adjusted based on the distance r_i $\{\forall\ i \in (\mathrm{M,S})\}$[4] between ν and iBS [3]. The power received by a iBS can be written as $P_{r,i} = P^{U_L}_{t,\nu} r_i^{\alpha\epsilon}$, where $P^{U_L}_{t,\nu}$ is the UTP of ν [8]. Hence, the U_L power received by iBS from ν at a distance r_i can be expressed as $P^{U_L}_{r,i} = P^{U_L}_{t,\nu} r_i^{\alpha\epsilon} |h_{i,\nu}| r_i^{-\alpha} = P^{U_L}_{t,\nu} |h_{i,\nu}| r_{i,\nu}^{\alpha(\epsilon-1)}$, where $r_i^{-\alpha}$ is the propagation path loss. Several plausible cases for various values of ϵ are described as follows.

1) $\boldsymbol{\epsilon = 0}$: UTP does not dynamically change with respect to r_i between ν and iBS, hence, UTP is assumed to be fixed. Thus, in this case, there is no U_L power control. Therefore, the ν located at the edge of iBS receives low power while the ν near iBS receives high power.
2) $\boldsymbol{\epsilon = 1}$: In this case, the U_L power received by iBS becomes irrelevant to r_i due to complete path loss compensation. Hence, the U_L received power by iBS from all the associated users will be the same, irrespective of their distances from iBS.
3) $\boldsymbol{0 < \epsilon < 1}$: In this case, the path loss is partially compensated by FPC. Increasing ϵ leads to improved iBS edge users' received power, however, ICI also increases. Similarly, lower ϵ results in reduced edge users' received power and, thus, leads to lower ICI.

C. UNIFORM AND NON-UNIFORM SBS DEPLOYMENT

In U-SBS$_{\mathcal{D}}$, SBSs are uniformly distributed throughout the coverage region of MBS [5]. U-SBS$_{\mathcal{D}}$ leads to severe ICI due to the SBS deployment near high transmitting power MBS and, thus, limits the network performance [9].

According to NU-SBS$_{\mathcal{D}}$, the coverage region of MBS is split into non-intersecting regions, i.e., center region, A^c_{M}, and outer region, A^o_{M}, with radii d_1 and d_2, respectively, [13], [14] (see Fig. 1b). SBSs are assumed to be distributed only in A^o_{M} using PHP, while locations of MBSs and users are modeled using IHPPPs. NU-SBS$_{\mathcal{D}}$ leads to improved edge user coverage by mitigating the interference.

D. REVERSE FREQUENCY ALLOCATION

For interference mitigation, traditional cellular networks follow frequency division duplex [9]. However, frequency reuse factor of unity is used in HetNets to achieve high throughput. This, however, increases ICI if both tiers operate simultaneously. Using the separate sub-bands for both U_L and D_L leads to improved spectral efficiency. Moreover, proactive interference management scheme is required to mitigate severe ICI. Therefore, we use RFA with NU-SBS$_{\mathcal{D}}$ and FPC to increase spectral efficiency in order to lower the interference. According to RFA, different sub-bands are assigned to MBSs and SBSs in A^g_{M} $\forall\ g \in (c, o)$, as indicated in Fig. 2, where c and o imply the center and outer region of MBS. Here, $\mathcal{F}_1$ and $\mathcal{F}_2$ denote the MBS sub-bands that are used in A^o_{M} and A^c_{M}, respectively. Moreover, $\mathcal{F}'_1$ and $\mathcal{F}'_2$ are the SBS sub-bands that are used in reverse directions and alternate regions, i.e., SBS outer region, A^o_{S}, and SBS center region, A^c_{S}, respectively. Such resource partitioning based on RFA leads to improved coverage and low interference due to efficient resource utilization.

III. ANALYSIS OF COVERAGE PROBABILITY

In this section, the coverage probability expressions are evaluated while assuming the ν located in A^c_{M} and A^o_{M} for the following network scenarios: (i) U_L coverage for U-SBS$_{\mathcal{D}}$

[4] M implies MBS and S implies SBS.

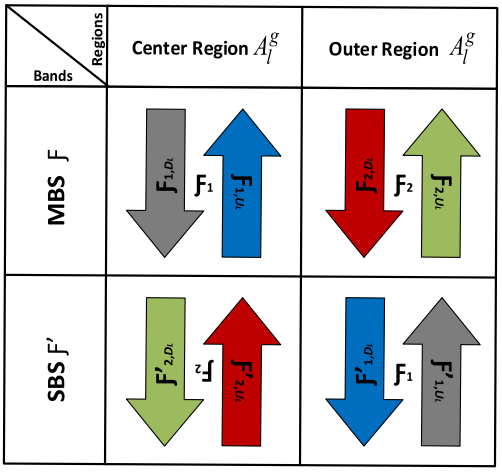

FIGURE 2. RFA employment mechanism.

with RFA and FPC, and (ii) U_L coverage for NU-SBS$_\mathcal{D}$ with RFA and FPC.

A. U_L COVERAGE ANALYSIS FOR U-SBS$_\mathcal{D}$ WITH RFA AND FPC

In U-SBS$_\mathcal{D}$, we uniformly deploy SBSs throughout the region along with RFA and FPC to mitigate ICI. U-SBS$_\mathcal{D}$ is shown in Fig. 1a. The U_L coverage probability, $P^{cov}_{A_i^c,U_L}(\beta_\nu)$, for U-SBS$_\mathcal{D}$ with RFA while considering the ν in A_i^c can be written as

$$P^{cov}_{A_i^c,U_L}(\beta_\nu) = P\left(\mathrm{SIR}_i^{U_L} > \beta_\nu\right). \tag{4}$$

Here, β_ν denotes SIR threshold while $\mathrm{SIR}_i^{U_L}$ represents the U_L SIR received by iBS from the ν. $\mathrm{SIR}_i^{U_L}$ from (4) can be rewritten as

$$\begin{aligned}\mathrm{SIR}_i^{U_L} &= \frac{P^{U_L}_{t,\nu}|h_{i,\nu}|r_{i,\nu}^{\alpha(\epsilon-1)}}{I^{U_L}_{\phi_{\tau,\nu},A_i^c}+I^{D_L}_{\phi_i,A_i^o}}\\ &= \frac{P^{U_L}_{t,\nu}|h_{i,\nu}|r_{i,\nu}^{\alpha(\epsilon-1)}}{\sum\limits_{j\in\phi_{\tau,\nu}}P^{t,U_L}_j|h_j|r_j^{\alpha(\epsilon-1)}+\sum\limits_{k\in\phi_i}P^{t,D_L}_k|h_k|r_k^{-\alpha}}.\end{aligned} \tag{5}$$

Here, $i\in\{\mathrm{M},\mathrm{S}\}$ and $\tau\in\{\mathrm{M},\mathrm{S}\}\ \forall\ i\neq\tau$, simultaneously. $P^{U_L}_{t,\nu}$ is the U_L transmit power of MBS-AUs.

According to RFA, the interference received in U_L is due to both U_L and D_L interferences from MBS-tier in A_i^c, i.e., $I^{U_L}_{\phi_{\tau,\nu},A_i^c}$, and D_L interference from SBS-tier in A_i^o, i.e., $I^{D_L}_{\phi_i,A_i^o}$. Therefore,

$$\begin{aligned}&P^{cov}_{A_i^c,U_L}(\beta_\nu)\\ &\overset{(1)}{=} P\left(\frac{P^{U_L}_{t,\nu}|h_{i,\nu}|r_{i,\nu}^{\alpha(\epsilon-1)}}{I^{U_L}_{\phi_{\tau,\nu},A_i^c}+I^{D_L}_{\phi_i,A_i^o}}>\beta_\nu\right)\\ &\overset{(2)}{=} \mathrm{E}_{r_i,I^{U_L}_{\phi_{\tau,\nu},A_i^c},I^{D_L}_{\phi_i,A_i^o}}\left[\exp\left(-\frac{r_{i,\nu}^{-\alpha(\epsilon-1)}\beta_\nu}{P^{U_L}_{t,\nu}}\left(I^{U_L}_{\phi_{\tau,\nu},A_i^c}+I^{D_L}_{\phi_i,A_i^o}\right)\right)\right]\\ &\overset{(3)}{=} \mathrm{E}_{r_i,I^{U_L}_{\phi_{\tau,\nu},A_i^c},I^{D_L}_{\phi_i,A_i^o}}\left[\exp\left(-s\left(I^{U_L}_{\phi_{\tau,\nu},A_i^c}+I^{D_L}_{\phi_i,A_i^o}\right)\right)\right]\\ &\overset{(4)}{=} \mathrm{E}_{r_i}\left[\mathrm{E}_{I^{U_L}_{\phi_{\tau,\nu},A_i^c}}\left(\exp\left(-s\left(I^{U_L}_{\phi_{\tau,\nu},A_i^c}\right)\right)\right)\right.\\ &\qquad\left.\times\mathrm{E}_{I^{D_L}_{\phi_i,A_i^o}}\left(\exp\left(-s\left(I^{D_L}_{\phi_i,A_i^o}\right)\right)\right)\right]\\ &\overset{(5)}{=} \mathrm{E}_{r_i}\left[\mathcal{L}_{I^{U_L}_{\phi_{\tau,\nu},A_i^c}}(s)\times\mathcal{L}_{I^{D_L}_{\phi_i,A_i^o}}(s)\right].\end{aligned} \tag{6}$$

In (6), Step (1) is achieved by using the coverage probability definition [2], [9]. Step (2) follows from Step (1) (see Appendix). Similarly, Step (3) is achieved by substituting $s=\left(r_{i,\nu}^{-\alpha(\epsilon-1)}\beta_\nu\right)/\left(P^{U_L}_{t,\nu}\right)$ into Step (2). Step (4) follows from the exponential property of sums into products. Finally, Step (5) follows from Step (4) through Laplace transform (LT) definition [9].

1) U_L COVERAGE ANALYSIS FOR MBS-ASSOCIATED ν IN A^c_M WHILE CONSIDERING U-SBS$_\mathcal{D}$ WITH RFA AND FPC

The coverage probability expression, $P^{cov}_{A^c_\mathrm{M},U_L}(\beta_\nu)$, for MBS-associated ν in A^c_M while considering U-SBS$_\mathcal{D}$ with RFA and FPC can be obtained as

$$\begin{aligned}&P^{cov}_{A^c_\mathrm{M},U_L}(\beta_\nu)\\ &=\mathrm{E}_{r_{\mathrm{M},\nu}}\left[\mathcal{L}_{I^{U_L}_{\phi_{\mathrm{M},\nu},A^c_\mathrm{M}}}(s)\times\mathcal{L}_{I^{D_L}_{\phi_\mathrm{S},A^o_\mathrm{M}}}(s)\right]\Big|_{s=\frac{r_{\mathrm{M},\nu}^{-\alpha(\epsilon-1)}\beta_\nu}{P^{U_L}_{t,\nu}}}.\end{aligned} \tag{7}$$

The LT of the U_L interference from MBS-AUs in A^c_M, $\mathcal{L}_{I^{U_L}_{\phi_{\mathrm{M},\nu},A^c_\mathrm{M}}}(s)$, is obtained as

$$\begin{aligned}&\mathcal{L}_{I^{U_L}_{\phi_{\mathrm{M},\nu},A^c_\mathrm{M}}}(s)\\ &\overset{(a)}{=}\mathrm{E}_{I^{U_L}_{\phi_{\mathrm{M},\nu},A^c_\mathrm{M}}}\left[\exp\left(-I^{U_L}_{\phi_{\mathrm{M},\nu},A^c_\mathrm{M}}s\right)\right]\Big|_{s=\frac{r_{\mathrm{M},\nu}^{\alpha(1-\epsilon)}\beta_\nu}{P^{U_L}_{t,\nu}}}\\ &\overset{(b)}{=}\mathrm{E}_{I^{U_L}_{\phi_{\mathrm{M},\nu},A^c_\mathrm{M}},|h_j|}\left[\exp\left(-s\sum_{j\in\phi_{\mathrm{M},\nu}}P^{U_L}_{t,\nu}|h_j|r_j^{\alpha(\epsilon-1)}\right)\right]\\ &\overset{(c)}{=}\mathrm{E}_{I^{U_L}_{\phi_{\mathrm{M},\nu},A^c_\mathrm{M}},|h_j|}\left[\prod_{j\in\phi_{\mathrm{M},\nu}}\exp\left(-|h_j|\beta_\nu r_{\mathrm{M},\nu}^{-\alpha(\epsilon-1)}r_j^{\alpha(\epsilon-1)}\right)\right]\\ &\overset{(d)}{=}\mathrm{E}_{I^{U_L}_{\phi_{\mathrm{M},\nu},A^c_\mathrm{M}}}\left[\prod_{j\in\phi_{\mathrm{M},\nu}}\mathrm{E}_{|h_j|}\left(\exp\left(-|h_j|\beta_\nu r_{\mathrm{M},\nu}^{-\alpha(\epsilon-1)}r_j^{\alpha(\epsilon-1)}\right)\right)\right]\\ &\overset{(e)}{=}\mathrm{E}_{I^{U_L}_{\phi_{\mathrm{M},\nu},A^c_\mathrm{M}}}\left[\prod_{j\in\phi_{\mathrm{M},\nu}}\frac{1}{1+\beta_\nu\left(\frac{r_j}{r_{\mathrm{M},\nu}}\right)^{\alpha(\epsilon-1)}}\right]\end{aligned}$$

$$\overset{(f)}{=} \exp\left(-2\pi\lambda_{\mathrm{M},\nu}\int_{y}^{d_1}\frac{r_j dr_j}{1+\left(\frac{r_j}{\beta_\nu^{\frac{1}{\alpha(1-\epsilon)}}r_{\mathrm{M},\nu}}\right)^{\alpha(1-\epsilon)}}\right)$$

$$\overset{(g)}{=} \exp\left(-\frac{\pi\lambda_{\mathrm{M},\nu}r_{\mathrm{M},\nu}^2}{\beta_\nu^{\frac{-2}{\alpha(1-\epsilon)}}}\int_{\left(\frac{y}{\beta_\nu^{\frac{1}{\alpha(1-\epsilon)}}r_{\mathrm{M},\nu}}\right)^2}^{\left(\frac{d_1}{\beta_\nu^{\frac{1}{\alpha(1-\epsilon)}}r_{\mathrm{M},\nu}}\right)^2}\frac{du}{1+(u)^{\frac{\alpha(1-\epsilon)}{2}}}\right)$$

$$\overset{(h)}{\approx} \exp\Bigg(\frac{2\pi\lambda_{\mathrm{M},\nu}r_{\mathrm{M},\nu}^{\alpha(1-\epsilon)}y^{2+\alpha(\epsilon-1)}\beta_\nu}{2+\alpha(\epsilon-1)}\,{}_2F_1\left(1,1+\frac{2}{\alpha(\epsilon-1)},2+\frac{2}{\alpha(\epsilon-1)},-\frac{y^{\alpha(\epsilon-1)}\beta_\nu}{r_{\mathrm{M},\nu}^{\alpha(\epsilon-1)}}\right)$$
$$-\frac{2\pi\lambda_{\mathrm{M},\nu}r_{\mathrm{M},\nu}^{\alpha(1-\epsilon)}d_1^{2+\alpha(\epsilon-1)}\beta_\nu}{2+\alpha(\epsilon-1)}\,{}_2F_1\left(1,1+\frac{2}{\alpha(\epsilon-1)},2+\frac{2}{\alpha(\epsilon-1)},-\frac{d_1^{\alpha(\epsilon-1)}\beta_\nu}{r_{\mathrm{M},\nu}^{\alpha(\epsilon-1)}}\right)\Bigg). \tag{8}$$

In (8), Step (a) followed from the definition of LT [9], Step (b) is achieved by replacing $I^{U_L}_{\phi_{\mathrm{M},\nu},A^c_{\mathrm{M}}} = \sum_{j\in\phi_{\mathrm{M},\nu}}P^{U_L}_{t,\nu}|h_j|r_j^{\alpha(\epsilon-1)}$, into Step (a), Step (c) is achieved by replacing $s = \left(r_{i,\nu}^{-\alpha(\epsilon-1)}\beta_\nu\right)/\left(P^{U_L}_{t,\nu}\right)$ into Step (b), Step (e) follows from the LT of Step (d) with respect to h_j, Step (f) is achieved by using the probability generating functional (PGFL) of IHPPP [29], Step (g) is achieved by replacing $u = \left(r_j/(\beta_\nu)^{1/\alpha(\epsilon-1)}r_{\mathrm{M},\nu}\right)^2$ into Step (f), and Step (h) is achieved by following Gauss-hypergeometric approximation of Step (e) [31].

By applying the similar procedure as used for (8), the LT of the U_L interference from MBS-AUs in A^o_{M}, $\mathcal{L}_{I^{U_L}_{\phi_{\mathrm{M},\nu},A^o_{\mathrm{M}}}}(s)$, is obtained as

$$\mathcal{L}_{I^{U_L}_{\phi_{\mathrm{M},\nu},A^o_{\mathrm{M}}}}(s) = \exp\Bigg(\frac{2\pi\lambda_{\mathrm{M},\nu}r_{\mathrm{M},\nu}^{\alpha(1-\epsilon)}d_1^{2+\alpha(\epsilon-1)}\beta_\nu}{2+\alpha(\epsilon-1)}\times{}_2F_1\left(1,1+\frac{2}{\alpha(\epsilon-1)},2+\frac{2}{\alpha(\epsilon-1)},-d_1^{\alpha(\epsilon-1)}r_{\mathrm{M},\nu}^{\alpha(1-\epsilon)}\beta_\nu\right)$$
$$-\frac{2\pi\lambda_{\mathrm{M},\nu}r_{\mathrm{M},\nu}^{\alpha(1-\epsilon)}d_2^{2+\alpha(\epsilon-1)}\beta_\nu}{2+\alpha(\epsilon-1)}\times{}_2F_1\left(1,1+\frac{2}{\alpha(\epsilon-1)},2+\frac{2}{\alpha(\epsilon-1)},-d_2^{\alpha(\epsilon-1)}r_{\mathrm{M},\nu}^{\alpha(1-\epsilon)}\beta_\nu\right)\Bigg). \tag{11}$$

The LT of the D_L interference from SBSs in A^o_{M}, $\mathcal{L}_{I^{D_L}_{\phi_{\mathrm{S}},A^o_{\mathrm{M}}}}(s)$, is written as

$$\mathcal{L}_{I^{D_L}_{\phi_{\mathrm{S}},A^o_{\mathrm{M}}}}(s) \overset{(i)}{=} \mathrm{E}_{I^{D_L}_{\phi_{\mathrm{S}},A^o_{\mathrm{M}}}}\left[\exp\left(-I^{D_L}_{\phi_{\mathrm{S}},A^o_{\mathrm{M}}}s\right)\right]\Big|_{s=\frac{r_{\mathrm{M},\nu}^{-\alpha(\epsilon-1)}\beta_\nu}{P^{U_L}_{t,\nu}}}$$
$$\overset{(j)}{=} \mathrm{E}_{I^{D_L}_{\phi_{\mathrm{S}},A^o_{\mathrm{M}}},|h_k|}\left[\exp\left(-s\sum_{k\in\phi_{\mathrm{S}}}P^{D_L}_{\mathrm{S}}|h_k|r_k^{-\alpha}\right)\right]$$
$$\overset{(k)}{=} \mathrm{E}_{I^{D_L}_{\phi_{\mathrm{S}},A^o_{\mathrm{M}}},|h_k|}\left[\prod_{k\in\phi_{\mathrm{S}}}\exp\left(-|h_k|\eta_1\beta_\nu r_{\mathrm{M},\nu}^{-\alpha(\epsilon-1)}r_k^{-\alpha}\right)\right]$$
$$\overset{(l)}{=} \mathrm{E}_{I^{D_L}_{\phi_{\mathrm{S}},A^o_{\mathrm{M}}}}\left[\prod_{k\in\phi_{\mathrm{S}}}\mathrm{E}_{|h_k|}\left(\exp\left(-|h_k|\eta_1\beta_\nu r_{\mathrm{M},\nu}^{-\alpha(\epsilon-1)}r_k^{-\alpha}\right)\right)\right]$$
$$\overset{(m)}{=} \mathrm{E}_{I^{D_L}_{\phi_{\mathrm{S}},A^o_{\mathrm{M}}}}\left[\prod_{k\in\phi_{\mathrm{S}}}\frac{1}{1+\eta_1\beta_\nu\left(r_{\mathrm{M},\nu}^{(\epsilon-1)}r_k\right)^{-\alpha}}\right]$$

$$P^{cov}_{A^c_{\mathrm{M}},U_L}(\beta_\nu) = \frac{2\pi\lambda_{\mathrm{M},\nu}}{1-\exp\left(-\lambda_{\mathrm{M}}\pi d_1^2\right)}\int_y^{d_1}\exp\Bigg(2\pi\lambda_{\mathrm{M},\nu}r_{\mathrm{M},\nu}^{\alpha(1-\epsilon)}\Bigg[\frac{y^{2+\alpha(\epsilon-1)}\beta_\nu}{2+\alpha(\epsilon-1)}\mathcal{J}\left(\alpha\epsilon,-\frac{y^{\alpha(\epsilon-1)}\beta_\nu}{r_{\mathrm{M},\nu}^{\alpha(\epsilon-1)}}\right)-\frac{d_1^{2+\alpha(\epsilon-1)}\beta_\nu}{2+\alpha(\epsilon-1)}$$
$$\times\,\mathcal{J}\left(\alpha\epsilon,-d_1^{\alpha(\epsilon-1)}r_{\mathrm{M},\nu}^{\alpha(1-\epsilon)}\beta_\nu\right)-\frac{\lambda_{\mathrm{S}}\eta_1 d_1^{2-\alpha}\beta_\nu}{2\lambda_{\mathrm{M},\nu}(\frac{\alpha}{2}-1)}\mathcal{J}\left(\alpha,-d_1^{-\alpha}r_{\mathrm{M},\nu}^{\alpha(1-\epsilon)}\beta_\nu\eta_1\right)-\frac{\lambda_{\mathrm{M},\nu}r_{\mathrm{M},\nu}^2}{2\,r_{\mathrm{M},\nu}^{\alpha(1-\epsilon)}}\Bigg]\Bigg)r_{\mathrm{M},\nu}dr_{\mathrm{M},\nu}. \tag{9}$$

$$P^{cov}_{A^o_{\mathrm{M}},U_L}(\beta_\nu) = \frac{2\pi\lambda_{\mathrm{M},\nu}}{\exp\left(-\lambda_{\mathrm{M}}\pi d_1^2\right)}\int_{d_1}^{d_2}\exp\Bigg(2\pi\lambda_{\mathrm{S}}\beta_\nu r_{\mathrm{M},\nu}^{\alpha(1-\epsilon)}\eta_1\Bigg[\frac{d_1^{2-\alpha}}{\alpha-2}\mathcal{J}\left(\alpha,-\frac{\beta_\nu\eta_1}{d_1^\alpha r_{\mathrm{M},\nu}^{\alpha(\epsilon-1)}}\right)-\frac{X_1^{2-\alpha}}{\alpha-2}\mathcal{J}\left(\alpha,-\frac{\beta_\nu\eta_1}{X_1^\alpha r_{\mathrm{M},\nu}^{\alpha(\epsilon-1)}}\right)$$
$$+\frac{\lambda_{\mathrm{M},\nu}d_1^{2+\alpha(\epsilon-1)}}{\eta_1\lambda_{\mathrm{S}}(2+\alpha(\epsilon-1))}\mathcal{J}\left(\alpha\epsilon,-\frac{d_1^{\alpha(\epsilon-1)}\beta_\nu}{r_{\mathrm{M},\nu}^{\alpha(\epsilon-1)}}\right)-\frac{\lambda_{\mathrm{M},\nu}r_{\mathrm{M},\nu}^2}{2\lambda_{\mathrm{S}}\eta_1\beta_\nu r_{\mathrm{M},\nu}^{\alpha(1-\epsilon)}}-\frac{\lambda_{\mathrm{M},\nu}d_2^{2+\alpha(\epsilon-1)}}{\eta_1\lambda_{\mathrm{S}}(2+\alpha(\epsilon-1))}\mathcal{J}\left(\alpha\epsilon,-\frac{d_2^{\alpha(\epsilon-1)}\beta_\nu}{r_{\mathrm{M},\nu}^{\alpha(\epsilon-1)}}\right)\Bigg]\Bigg)r_{\mathrm{M},\nu}dr_{\mathrm{M},\nu}. \tag{10}$$

$$\overset{(n)}{=} \exp\left(-2\pi\lambda_S \int_{d_1}^{d_2} \frac{r_k dr_k}{1+\left(\frac{r_{M,v}^{(\epsilon-1)} r_k}{(\eta_1\beta_v)^{1/\alpha}}\right)^{\alpha}}\right)$$

$$\overset{(o)}{=} \exp\left(\frac{-\pi\lambda_S(\beta_v\eta_1)^{2/\alpha}}{r_{M,v}^{2(\epsilon-1)}} \int_{\left(\frac{r_{M,v}^{\epsilon-1} d_1}{(\eta_1\beta_v)^{1/\alpha}}\right)^2}^{\left(\frac{r_{M,v}^{\epsilon-1} d_2}{(\eta_1\beta_v)^{1/\alpha}}\right)^2} \frac{du}{1+(u)^{\frac{\alpha}{2}}}\right)$$

$$\overset{(p)}{\approx} \exp\Bigg(\frac{\pi\lambda_S d_2^{(2-\alpha)} r_{M,v}^{\alpha(1-\epsilon)}\beta_v\eta_1}{\alpha/2-1} \times {}_2F_1\left(1,1-\frac{2}{\alpha},2-\frac{2}{\alpha},-d_2^{-\alpha} r_{M,v}^{\alpha(1-\epsilon)}\beta_v\eta_1\right) - \frac{\pi\lambda_S d_1^{(2-\alpha)} r_{M,v}^{\alpha(1-\epsilon)}\beta_v\eta_1}{\alpha/2-1} \times {}_2F_1\left(1,1-\frac{2}{\alpha},2-\frac{2}{\alpha},-d_1^{-\alpha} r_{M,v}^{\alpha(1-\epsilon)}\beta_v\eta_1\right)\Bigg). \quad (12)$$

In (12), Step (i) is achieved from the LT definition [9], Step (j) is achieved by replacing $I^{U_L}_{\phi_{M,v},A_M^c} = \sum_{j\in\phi_{M,v}} P^{U_L}_{t,v}|h_j| r_j^{\alpha(\epsilon-1)}$ into Step (i), Step (k) is achieved by replacing $s = \left(r_{i,v}^{-\alpha(\epsilon-1)}\beta_v\right) / \left(P^{U_L}_{t,v}\right)$ into Step (j), Step (m) is achieved by evaluating the LT of Step (l) with respect to h_j, Step (n) is achieved by using the PGFL of IHPPP [29], Step (o) is achieved by replacing $u = \left(r_{M,v}^{(\epsilon-1)} r_k / (\eta_1\beta_v)^{1/\alpha}\right)^2$ into Step (n), and Step (p) is achieved by following the Gauss-hypergeometric approximation of Step (m) [31]. Moreover, $\eta_1 = P_S^{D_L}/P_{t,v}^{U_L}$, where $P_S^{D_L}$ is the SBSs transmit power in D_L.

Furthermore, the LT of the D_L interference from SBS in A_M^c, $\mathcal{L}_{I^{D_L}_{\phi_S,A_M^c}}(s)$, is obtained as

$$\mathcal{L}_{I^{D_L}_{\phi_S,A_M^c}}(s) = \exp\Bigg[\Bigg(\frac{\pi\lambda_S d_1^{(2-\alpha)} r_{M,v}^{\alpha(1-\epsilon)}\beta_v\eta_1}{\alpha/2-1} \times {}_2F_1\left(1,1-\frac{2}{\alpha},2-\frac{2}{\alpha},-d_1^{-\alpha} r_{M,v}^{\alpha(1-\epsilon)}\beta_v\eta_1\right)\Bigg) - \Bigg(\frac{\pi\lambda_S X^{(2-\alpha)} r_{M,v}^{\alpha(1-\epsilon)}\beta_v\eta_1}{\alpha/2-1} \times {}_2F_1\left(1,1-\frac{2}{\alpha},2-\frac{2}{\alpha},-X^{-\alpha} r_{M,v}^{\alpha(1-\epsilon)}\beta_v\eta_1\right)\Bigg)\Bigg]. \quad (13)$$

In (13), X is the distance between the SBS and its nearest associated v. Moreover, v located in A_M^c and A_M^o while associated with MBS at a distance $r_{M,v}$, has PDFs given, respectively, as

$$f_{r_{M,v}|U_{A_M^c}}(r_{M,v}) = \frac{2\pi\lambda_{M,v} r_{M,v}\exp\left(-\lambda_{M,v}\pi r_{M,v}^2\right)}{1-\exp\left(-\lambda_M\pi d_1^2\right)}, \quad (16)$$

and

$$f_{r_{M,v}|U_{A_M^o}}(r_{M,v}) = \frac{2\pi\lambda_{M,v} r_{M,v}\exp\left(-\lambda_{M,v}\pi r_{M,v}^2\right)}{\exp\left(-\lambda_M\pi d_1^2\right)}. \quad (17)$$

The coverage probability expression of U-SBS$_\mathcal{D}$ for the MBS-associated v in A_M^c for U-SBS$_\mathcal{D}$ with RFA, $P^{cov}_{A_M^c}(\beta_v)$, can be written as [5], [24]

$$P^{cov}_{A_M^c,U_L}(\beta_v) = \int_y^{d_1} \mathcal{L}_{I^{U_L}_{\phi_{M,v},A_M^c}}(s)\, \mathcal{L}_{I^{D_L}_{\phi_S,A_M^o}}(s) f_{r_{M,v}|U_{A_M^c}}(r_{M,v})\, dr_{M,v}. \quad (18)$$

Now, substituting (8), (12), and (16) into (18), we obtain $P^{cov}_{A_M^c,U_L}(\beta_v)$ as (9), as shown at the bottom of the previous page. In (9), $\mathcal{J}(\cdot)$ denotes the Gauss-hypergeometric function (the same applies in the rest of the paper).

2) U_L COVERAGE ANALYSIS FOR MBS-ASSOCIATED v IN A_M^o WHILE CONSIDERING U-SBS$_\mathcal{D}$ WITH RFA AND FPC

The coverage probability expression, $P^{cov}_{A_M^o,U_L}(\beta_v)$, for the MBS-associated v in A_M^o while considering U-SBS$_\mathcal{D}$ with RFA and FPC can be obtained as

$$P^{cov}_{A_M^o,U_L}(\beta_v) = \int_{d_1}^{d_2} \mathcal{L}_{I^{U_L}_{\phi_{M,v},A_M^o}}(s)\, \mathcal{L}_{I^{D_L}_{\phi_S,A_M^c}}(s) f_{r_{M,v}|U_{A_M^o}}(r_{M,v})\, dr_{M,v}. \quad (19)$$

By substituting (11), (13), and (17) into (19), $P^{cov*}_{A_M^c,U_L}(\beta_v)$ can be written as (10), as shown at the bottom of previous page.

$$P^{cov*}_{A_M^c,U_L}(\beta_v) = \frac{2\pi\lambda_{M,v}}{1-\exp\left(-\lambda_M\pi d_1^2\right)} \int_y^{d_1} \exp\Bigg(2\pi\lambda_{M,v} r_{M,v}^{\alpha(1-\epsilon)} \Bigg[\frac{y^{2+\alpha(\epsilon-1)}\beta_v}{2+\alpha(\epsilon-1)} \mathcal{J}\left(\alpha\epsilon, -\frac{y^{\alpha(\epsilon-1)}\beta_v}{r_{M,v}^{\alpha(\epsilon-1)}}\right) - \frac{d_1^{2+\alpha(\epsilon-1)}\beta_v}{2+\alpha(\epsilon-1)} \times \mathcal{J}\left(\alpha\epsilon, -\frac{d_1{}^{\alpha(\epsilon-1)}\beta_v}{r_{M,v}^{\alpha(\epsilon-1)}}\right) - \frac{\lambda_S\exp(-\lambda_M\pi d_1^2)\eta_1\, d_1^{2-\alpha}\beta_v}{2\lambda_{M,v}(\frac{\alpha}{2}-1)} \mathcal{J}\left(\alpha, -\frac{\beta_v\eta_1}{d_1^\alpha r_{M,v}^{\alpha(\epsilon-1)}}\right) - \frac{\lambda_{M,v} r_{M,v}^2}{2\, r_{M,v}^{\alpha(1-\epsilon)}}\Bigg]\Bigg) r_{M,v} dr_{M,v}. \quad (14)$$

$$P^{cov*}_{A_M^o,U_L}(\beta_v) = \frac{2\pi\lambda_{M,v}}{\exp\left(-\lambda_M\pi d_1^2\right)} \int_{d_1}^{d_2} \exp\Bigg(\frac{2\pi\beta_v\lambda_{M,v} d_1^{2+\alpha(\epsilon-1)} r_{M,v}^{\alpha(1-\epsilon)}}{2+\alpha(\epsilon-1)} \mathcal{J}\left(\alpha\epsilon, -\frac{d_1{}^{\alpha(\epsilon-1)}\beta_v}{r_{M,v}^{\alpha(\epsilon-1)}}\right) - \pi\lambda_{M,v} r_{M,v}^2 - \frac{2\pi\beta_v\lambda_{M,v} d_2^{2+\alpha(\epsilon-1)} r_{M,v}^{\alpha(1-\epsilon)}}{2+\alpha(\epsilon-1)} \mathcal{J}\left(\alpha\epsilon, -\frac{d_2{}^{\alpha(\epsilon-1)}\beta_v}{r_{M,v}^{\alpha(\epsilon-1)}}\right)\Bigg) r_{M,v} dr_{M,v}. \quad (15)$$

TABLE 2. Simulation parameters.

Parameter	Configuration
MBS and SBS distribution	IHPPP
Code iterations	1000
ϵ	0 and 0.5
λ_{M}	$2 / \pi(1000\mathrm{m})^2$
λ_{S}	$10 / \pi(1000\mathrm{m})^2$
$P_{t,\mathrm{S}}^{\mathrm{DL}}$, $P_{t,\nu}^{\mathrm{UL}}$	30 dBm and 20 dBm, respectively
$\alpha_m = \alpha_s = \alpha$	$2 < \alpha \leq 4$

B. U_L COVERAGE ANALYSIS FOR NU-SBS$_{\mathcal{D}}$ WITH RFA AND FPC

In the NU-SBS$_{\mathcal{D}}$ scenario, we assume nonuniform deployment of SBSs in the MBS coverage area by following PHP together with RFA and FPC employment.

1) U_L COVERAGE PROBABILITY FOR MBS-ASSOCIATED ν IN A_{M}^c WHILE CONSIDERING NU-SBS$_{\mathcal{D}}$ WITH RFA AN D FPC

The coverage probability expression, $P^{cov*}_{A_{\mathrm{M}}^c,U_L}(\beta_\nu)$, for MBS-associated ν in A_{M}^c while considering NU-SBS$_{\mathcal{D}}$ with RFA and FPC is obtained as

$$P^{cov*}_{A_{\mathrm{M}}^c,U_L}(\beta_\nu)=\int_{d_1}^{d_2}\mathcal{L}_{I^{U_L}_{\phi_{\mathrm{M},\nu},A_{\mathrm{M}}^c}}(s)\,\mathcal{L}_{I^{D_L}_{\phi_{\mathrm{S}},A_{\mathrm{M}}^o}}(s)\,f_{r_{\mathrm{M},\nu}|U_{A_{\mathrm{M}}^c}}\left(r_{\mathrm{M},\nu}\right)dr_{\mathrm{M},\nu}. \tag{20}$$

By substituting (8), (12), and (16) into (20), $P^{cov*}_{A_{\mathrm{M}}^c,U_L}(\beta_\nu)$ can be given as (14), as shown at the bottom of the previous page.

2) U_L COVERAGE PROBABILITY FOR MBS-ASSOCIATED ν IN A_{M}^o WHILE CONSIDERING NU-SBS$_{\mathcal{D}}$ WITH RFA AND FPC

Coverage probability expression, $P^{cov*}_{A_{\mathrm{M}}^o,U_L}(\beta_\nu)$, for MBS-associated ν in A_{M}^o while considering NU-SBS$_{\mathcal{D}}$ with RFA and FPC can be written as

$$P^{cov*}_{A_{\mathrm{M}}^o,U_L}(\beta_\nu)=\int_{d_1}^{d_2}\mathcal{L}_{I^{U_L}_{\phi_{\mathrm{M},\nu}A_{\mathrm{M}}^o}}(s)\,f_{r_{\mathrm{M},\nu}|U_{A_{\mathrm{M}}^o}}\left(r_{\mathrm{M},\nu}\right)dr_{\mathrm{M},\nu}. \tag{21}$$

By substituting (11) and (17) into (21), $P^{cov*}_{A_{\mathrm{M}}^c,U_L}(\beta_\nu)$ is written as (15), as shown at the bottom of the previous page.

IV. RESULTS AND DISCUSSION

In this section, we discuss U_L coverage probability results for both U-SBS$_{\mathcal{D}}$ and NU-SBS$_{\mathcal{D}}$ models while assuming FPC and RFA. Results are derived from (9), (10), (14), and (15) using MATLAB (ver. 2017a). The analytical results are validated through Monte Carlo simulations using the parameters listed in Table 2. Moreover, the numerical analyses are obtained and validated through Mathematica (Ver. 11). Furthermore, the impact of different network parameters, such as β_ν, λ_{S}, ϵ, and $\frac{\lambda_{\mathrm{M},\nu}}{\lambda_{\mathrm{M}}}$, on U_L coverage is considered. All the results are drawn considering ν to be located in both A_{M}^c and A_{M}^o.

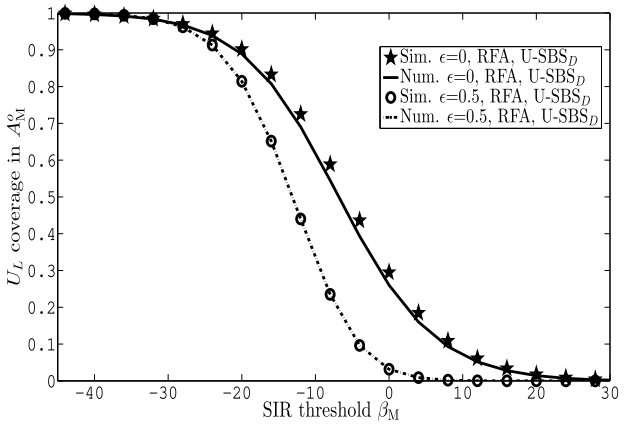

FIGURE 3. U_L coverage in A_{M}^o against β_{M}.

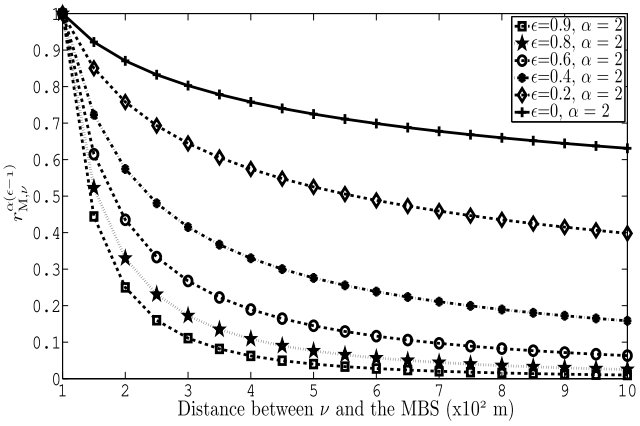

FIGURE 4. $r_{\mathrm{M}\nu}^{\alpha(\epsilon-1)}$ versus different values of distance between ν and the MBS.

Fig. 3 shows the numerical and simulation results for U_L coverage probabilities while considering U-SBS$_{\mathcal{D}}$. The plots are obtained for different values of ϵ and β_{M}. The results indicate that lower values of ϵ lead to higher U_L coverage due to lower U_L interference. Moreover, the plots in the figure show that higher values of β_{M} cause lower users association and, hence, lower U_L coverage.

Fig. 4 compares the values of path loss with FPC, $r_{\mathrm{M}\nu}^{\alpha(\epsilon-1)}$, against the distance between the ν and the associated MBS. The plots show that an increase in the distance between the ν and the MBS results in higher path loss. Moreover, increase in the value of ϵ leads to higher path loss compensation.

Fig. 5 depicts U_L coverage probability results, according to (9), against different values of β_ν and ϵ. Moreover, we assume that $\frac{\lambda_{\mathrm{M},\nu}}{\lambda_{\mathrm{M}}} = 2$ and ν is located in A_{M}^c. The results consider U-SBS$_{\mathcal{D}}$ model in conjunction with RFA and FPC. The plots demonstrate that higher values of ϵ provide reduced U_L coverage due to higher D_L interference received from SBSs in A_{M}^o. Hence, a multi-tier deployment results in reduced network performance gain when using FPC.

Fig. 6 presents U_L coverage probability, according to (10), against different values of β_ν and ϵ. We assume $\frac{\lambda_{\mathrm{M},\nu}}{\lambda_{\mathrm{M}}} = 2$ with the ν located in A_{M}^o. The results demonstrate that the U_L coverage in A_{M}^o degrades as compared with

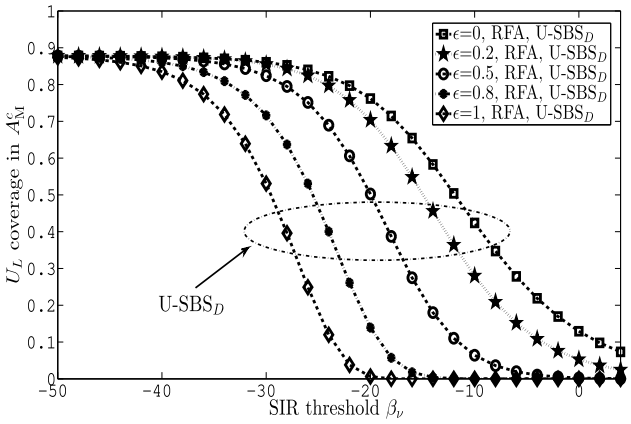

FIGURE 5. U_L coverage in A_{M}^{c} versus different values of β_ν, while using (9).

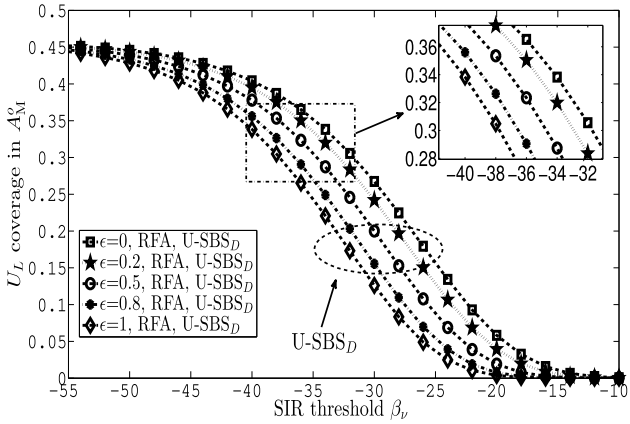

FIGURE 6. U_L coverage in A_{M}^{o} against different values of β_ν and ϵ, while using (10).

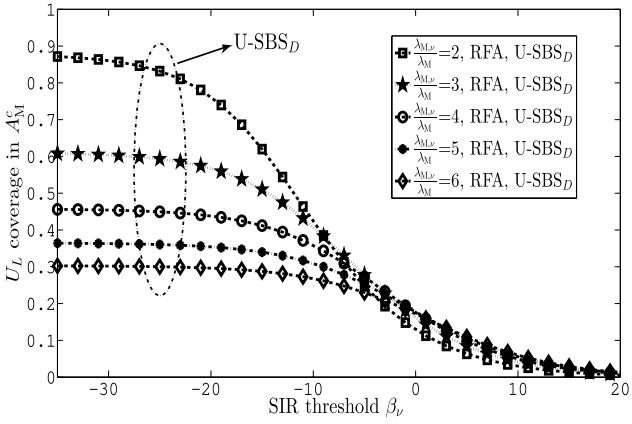

FIGURE 7. U_L coverage in A_{M}^{c} versus different values of β_ν and $\frac{\lambda_{\mathrm{M},\nu}}{\lambda_{\mathrm{M}}}$, while using (9).

A_{M}^{c} due to increase in the distance between the ν and the associated MBS. Moreover, an increase in the value of ϵ results in reduced coverage due to higher interference.

Fig. 7 shows U_L coverage probability, according to (9), against different values of $\frac{\lambda_{\mathrm{M},\nu}}{\lambda_{\mathrm{M}}}$ and β_ν. The plots indicate reduced U_L coverage due to increase in the value of $\frac{\lambda_{\mathrm{M},\nu}}{\lambda_{\mathrm{M}}}$.

In Fig. 8, we present U_L coverage probability, according to (10), against different values of ϵ and β_ν. The plots demon-

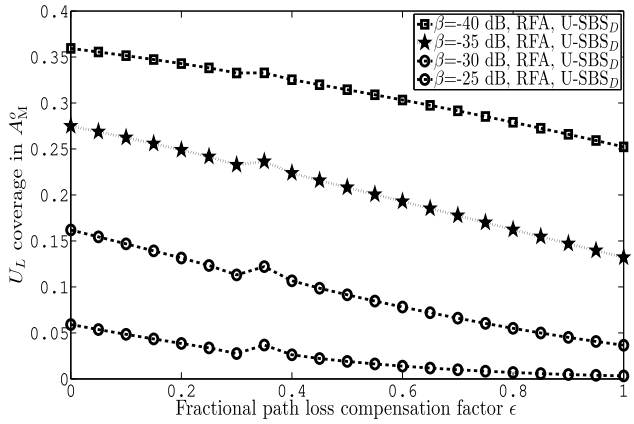

FIGURE 8. U_L coverage in A_{M}^{o} against different values of ϵ, while using (10).

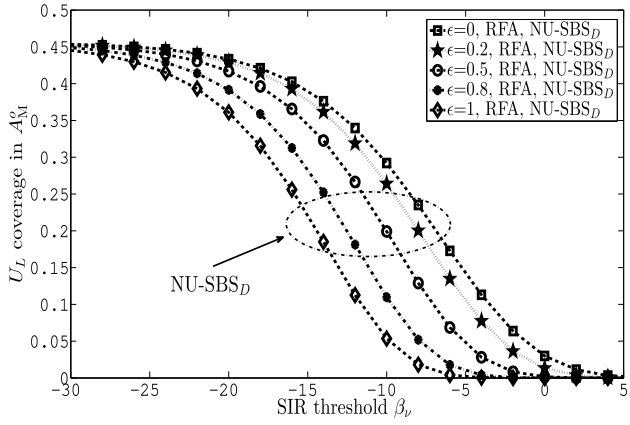

FIGURE 9. U_L coverage in A_{M}^{o} versus different values of β_ν and ϵ, while using (15).

strate that by increasing the value of ϵ, the U_L coverage is reduced due to higher received interference from SBSs located in A_{M}^{c}. Moreover, it can be observed that lower values of β_ν result in better U_L coverage. This is because of higher number of user associations with the MBS.

Furthermore, Fig. 9 presents U_L coverage probability, according to (15), against different values of β_ν and ϵ. The plots use NU-SBS$_{\mathcal{D}}$ model with $\frac{\lambda_{\mathrm{M},\nu}}{\lambda_{\mathrm{M}}} = 2$. The results depict lower U_L coverage with increase in the value of β_ν due to reduced number of user associations with MBS. Moreover, increasing the value of ϵ leads to reduced U_L coverage due to higher interference received from SBSs in A_{M}^{c}.

Fig. 10 describes U_L coverage probabilities, according to (10) and (15), while considering both U-SBS$_{\mathcal{D}}$ and NU-SBS$_{\mathcal{D}}$ models against different values of β_ν and ϵ in A_{M}^{o}. The plots demonstrate that NU-SBS$_{\mathcal{D}}$ model along with RFA and FPC provide improved U_L coverage in contrast to U-SBS$_{\mathcal{D}}$ model for different values of ϵ. Hence, our proposed model, i.e., NU-SBS$_{\mathcal{D}}$, improves the network performance gain.

Fig. 11 shows U_L coverage probabilities, according to (9) and (14), while considering both U-SBS$_{\mathcal{D}}$ and NU-SBS$_{\mathcal{D}}$ models against different values of β_ν and ϵ in A_{M}^{c}. We assume $\lambda_{\mathrm{S}} = 20$ and $\frac{\lambda_{\mathrm{M},\nu}}{\lambda_{\mathrm{M}}} = 2$. This result demonstrates that

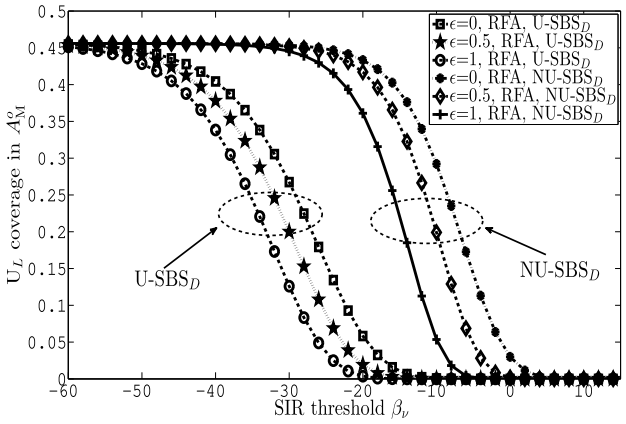

FIGURE 10. U_L coverage in A^o_M versus different values of β_ν and ϵ, while using (10) and (15).

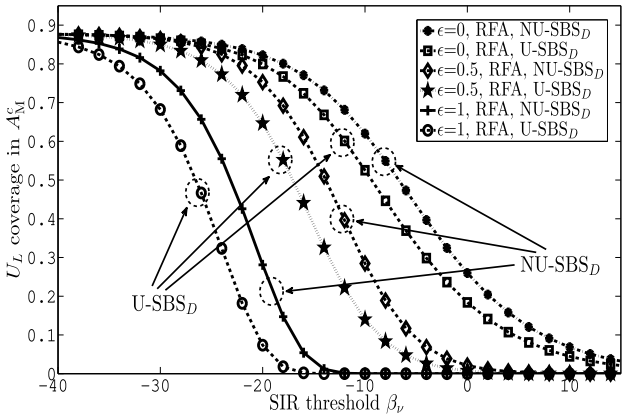

FIGURE 11. U_L coverage in A^c_M against β_ν and ϵ, while using (9) and (14).

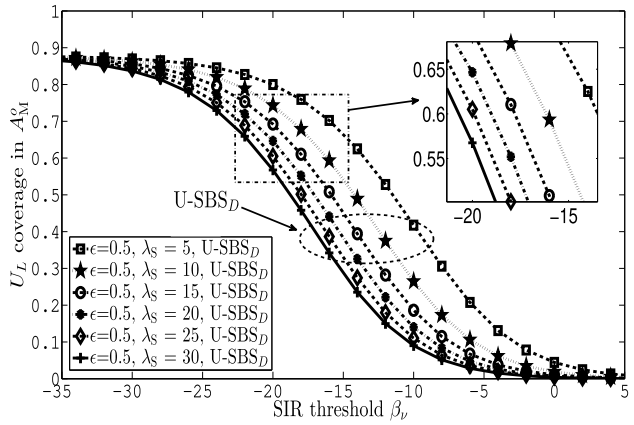

FIGURE 12. U_L coverage in A^c_M versus different values of λ_S, while using (9).

NU-SBS$_\mathcal{D}$ outperforms U-SBS$_\mathcal{D}$ in terms of coverage performance for all values of ϵ.

Fig. 12 compares U_L coverage probabilities, according to (9), against different values of λ_S and $\beta\nu$. The figure indicates degraded network performance with increasing values of λ_S due to significant interference.

Fig. 13 shows percentage U_L coverage improvement for different SIR threshold values by utilizing the data of Figs. 10 and 11. The plots in Fig. 13 show maximum U_L

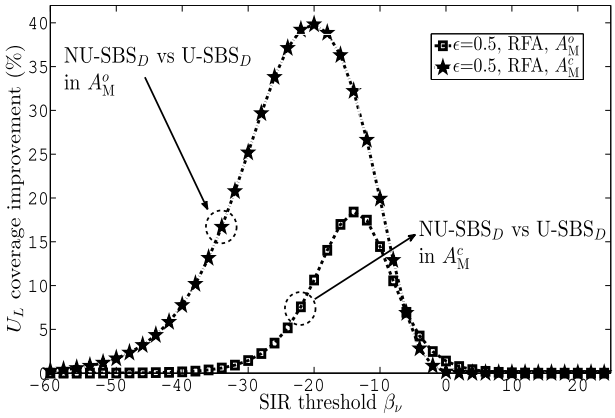

FIGURE 13. Percentage U_L coverage improvement versus different values of β_ν.

coverage improvement of 39.8 % in A^o_M when employing NU-SBS$_\mathcal{D}$ with FPC and RFA, as compared with U-SBS$_\mathcal{D}$ with FPC and RFA. Similarly, there is a maximum of 18.34 % U_L coverage improvement in A^c_M by employing the proposed model, i.e., NU-SBS$_\mathcal{D}$ with FPC and RFA.

V. CONCLUSION

In this paper, we have investigated U-SBS$_\mathcal{D}$ and NU-SBS$_\mathcal{D}$ models along with FPC and RFA. In HetNets, FPC is undesirable as it leads to significant increase in interference and, thus, limits network performance gain. Therefore, we have used NU-SBS$_\mathcal{D}$ model along with FPC and RFA to effectively abate ICI and, thus, leverage FPC in HetNets. The results indicate significant U_L coverage improvement with NU-SBS$_\mathcal{D}$ in conjunction with FPC and RFA, as compared with U-SBS$_\mathcal{D}$ in conjunction with FPC and RFA. Moreover, increasing the values of ϵ lowers the U_L coverage degradation for NU-SBS$_\mathcal{D}$ in contrast with U-SBS$_\mathcal{D}$. Hence, our proposed model is more resilient to ICI and, thus, provides enhanced edge users' coverage and leverages FPC in HetNets. As a future work, the proposed setup can be evaluated in conjunction with decoupled association to further mitigate the interference.

APPENDIX

PROOF OF STEP (2) IN (6)

Proof: By following the definition of coverage probability [2], we obtain $P^{cov}_{A^c_i,U_L}(\beta_\nu)$ as

$$P^{cov}_{A^c_i,U_L}(\beta_\nu) = P\left(\frac{P^{U_L}_{t,\nu}|h_{i,\nu}|r^{\alpha(\epsilon-1)}_{i,\nu}}{I^{U_L}_{\phi_{\tau,\nu},A^c_i} + I^{D_L}_{\phi_i,A^o_i}} > \beta_\nu\right). \quad (22)$$

with minor simplifications, we modify (22) as

$$P^{cov}_{A^c_i,U_L}(\beta_\nu) = P\left(|h_{i,\nu}| > \frac{r^{-\alpha(\epsilon-1)}_{i,\nu}\beta_\nu}{P^{U_L}_{t,\nu}}\left(I^{U_L}_{\phi_{\tau,\nu},A^c_i} + I^{D_L}_{\phi_i,A^o_i}\right)\right). \quad (23)$$

Now, by using (2.11) of [9], (23) modifies into Step (2) in (6).

REFERENCES

[1] M. A. Klatt, J. Lovrić, D. Chen, S. C. Kapfer, F. M. Schaller, P. W. A. Schönhöfer, B. S. Gardiner, A.-S. Smith, G. E. Schröder-Turk, and S. Torquato, "Universal hidden order in amorphous cellular geometries," *Nature Commun.*, vol. 10, no. 1, Dec. 2019, Art. no. 811.

[2] M. Arif, S. Wyne, and J. Ahmed, "Performance analysis of downlink and uplink decoupled access in clustered heterogeneous cellular networks," *Telecommun. Syst.*, vol. 72, no. 3, pp. 355–364, Nov. 2019.

[3] M. Coupechoux and J.-M. Kelif, "How to set the fractional power control compensation factor in LTE?" in *Proc. 34th IEEE Sarnoff Symp.*, May 2011, pp. 1–5.

[4] A. Nasser, O. Muta, M. Elsabrouty, and H. Gacanin, "Compressive sensing based spectrum allocation and power control for NOMA HetNets," *IEEE Access*, vol. 7, pp. 98495–98506, 2019.

[5] M. S. Haroon, Z. H. Abbas, F. Muhammad, and G. Abbas, "Analysis of coverage-oriented small base station deployment in heterogeneous cellular networks," *Phys. Commun.*, vol. 38, Feb. 2020, Art. no. 100908.

[6] X. Ge and W. Zhang, *Green Mobile Communication Networks*. Cham, Switzerland: Springer, 2019.

[7] S. Faruque, *Radio Frequency Multiple Access Techniques Made Easy*. Cham, Switzerland: Springer, 2019.

[8] R. Nikbakht and A. Lozano, "Uplink fractional power control for cell-free wireless networks," in *Proc. IEEE Int. Conf. Commun. (ICC)*, May 2019, pp. 1–5.

[9] B. Błaszczyszyn, M. Haenggi, P. Keeler, and S. Mukherjee, *Stochastic geometry analysis of cellular networks*. Cambridge, U.K.: Cambridge Univ. Press, 2018.

[10] Y. Zhang, Y. Liu, and J. Gao, "Decorrelating receiver of interference mitigation in MMwave small cells networks," *IEEE Access*, vol. 6, pp. 7772–7779, 2018.

[11] N. Al-Falahy and O. Alani, "Coverage and capacity improvement of millimetre wave 5G network using distributed base station architecture," *IET Netw.*, vol. 8, no. 4, pp. 246–255, Jul. 2019.

[12] W. Xu and H. Zhang, "Uplink interference mitigation for heterogeneous networks with user-specific resource allocation and power control," *EURASIP J. Wireless Commun. Netw.*, vol. 2014, no. 1, p. 55, Dec. 2014.

[13] S. Zou, N. Liu, Z. Pan, and X. You, "Joint power and resource allocation for non-uniform topologies in heterogeneous networks," in *Proc. IEEE 83rd Veh. Technol. Conf. (VTC Spring)*, May 2016, pp. 1–5.

[14] T. Han, J. Gong, X. Liu, S. M. R. Islam, Q. Li, Z. Bai, and K. S. Kwak, "On downlink NOMA in heterogeneous networks with non-uniform small cell deployment," *IEEE Access*, vol. 6, pp. 31099–31109, 2018.

[15] M. Fereydooni, M. Sabaei, M. Dehghan, G. Babazadeh Eslamlou, and M. Rupp, "Analytical evaluation of heterogeneous cellular networks under flexible user association and frequency reuse," *Comput. Commun.*, vol. 116, pp. 147–158, Jan. 2018.

[16] N. Naganuma, S. Nakazawa, S. Suyama, Y. Okumura, and H. Otsuka, "Performance evaluation of adaptive control CRE in HetNet with eICIC scheme," *IEICE Commun. Express*, vol. 6, no. 4, pp. 166–171, 2017.

[17] L. Guo, S. Cong, and Z. Sun, "Multichannel analysis of soft frequency reuse and user association in two-tier heterogeneous cellular networks," *EURASIP J. Wireless Commun. Netw.*, vol. 2017, no. 1, p. 168, Dec. 2017.

[18] F. Muhammad, Z. H. Abbas, G. Abbas, and L. Jiao, "Decoupled downlink-uplink coverage analysis with interference management for enriched heterogeneous cellular networks," *IEEE Access*, vol. 4, pp. 6250–6260, 2016.

[19] F. Muhammad, M. S. Haroon, Z. H. Abbas, G. Abbas, and S. Kim, "Uplink interference management for hetnets stressed by clustered wideband jammers," *IEEE Access*, vol. 7, pp. 182679–182690, 2019.

[20] Z. Zhang, R. Q. Hu, Y. Qian, and A. Papathanassiou, "D2D communication underlay in uplink cellular networks with fractional power control and fractional frequency reuse," in *Proc. IEEE Global Commun. Conf. (GLOBECOM)*, Dec. 2015, pp. 1–7.

[21] A. Haider, S.-H. Lee, S.-H. Hwang, D. I. Kim, and J. H. Na, "Uplink open loop power control for LTE HetNet," in *Proc. URSI Asia–Pacific Radio Sci. Conf. (URSI AP-RASC)*, Aug. 2016, pp. 83–85.

[22] W. Kim, Z. Kaleem, and K. Chang, "Interference-aware uplink power control in 3GPP LTE-A HetNet," *Wireless Pers. Commun.*, vol. 94, no. 3, pp. 1057–1071, 2017.

[23] M. M. Pervez, Z. H. Abbas, F. Muhammad, and L. Jiao, "Location-based coverage and capacity analysis of a two tier HetNet," *IET Commun.*, vol. 11, no. 7, pp. 1067–1073, May 2017.

[24] Z. H. Abbas, F. Muhammad, and L. Jiao, "Analysis of load balancing and interference management in heterogeneous cellular networks," *IEEE Access*, vol. 5, pp. 14690–14705, 2017.

[25] M. S. Haroon, Z. H. Abbas, G. Abbas, and F. Muhammad, "Coverage analysis of ultra-dense heterogeneous cellular networks with interference management," *Wireless Netw.*, vol. 26, no. 3, pp. 2013–2025, Apr. 2020.

[26] K.-H. Liu and T.-Y. Yu, "Performance of off-grid small cells with non-uniform deployment in two-tier HetNet," *IEEE Trans. Wireless Commun.*, vol. 17, no. 9, pp. 6135–6148, Sep. 2018.

[27] F. Muhammad, Z. H. Abbas, and F. Y. Li, "Cell association with load balancing in nonuniform heterogeneous cellular networks: Coverage probability and rate analysis," *IEEE Trans. Veh. Technol.*, vol. 66, no. 6, pp. 5241–5255, Jun. 2017.

[28] A. Ijaz, S. A. Hassan, S. A. R. Zaidi, D. N. K. Jayakody, and S. M. H. Zaidi, "Coverage and rate analysis for downlink HetNets using modified reverse frequency allocation scheme," *IEEE Access*, vol. 5, pp. 2489–2502, 2017.

[29] X. Jiang, B. Zheng, W.-P. Zhu, L. Wang, and Y. Zou, "Large system analysis of heterogeneous cellular networks with interference alignment," *IEEE Access*, vol. 6, pp. 8148–8160, 2018.

[30] M. Haenggi, *Stochastic Geometry for Wireless Networks*. Cambridge, U.K.: Cambridge Univ. Press, 2012.

[31] R. Hernandez-Aquino, S. A. R. Zaidi, D. McLernon, and M. Ghogho, "Modelling and performance evaluation of non-uniform two-tier cellular networks through stienen model," in *Proc. IEEE Int. Conf. Commun. (ICC)*, May 2016, pp. 1–6.

MUHAMMAD SAJID HAROON received the B.Sc. degree in electronics engineering from International Islamic University, Islamabad, Pakistan, in 2007, and the M.S. degrees in electrical engineering from the COMSATS Institute of Information Technology, Attock, Pakistan, in 2013. He is currently pursuing the Ph.D. degree with the Ghulam Ishaq Khan Institute of Engineering Sciences and Technology, Swabi, Pakistan, with a focus on interference management in next-generation cellular networks using tools from stochastic geometry, point process theory, and spatial statistics. His research interests include interference mitigation in cellular networks, next-generations cellular networks, stochastic processes, and digital signal processing.

FAZAL MUHAMMAD received the B.Sc. and M.Sc. degrees in electrical engineering from the University of Engineering and Technology, Peshawar, Pakistan, in 2004 and 2007, respectively, and the Ph.D. degree in electronic engineering from the GIK Institute of Engineering Sciences and Technology, Pakistan, in 2017. He is currently working as an Assistant Professor and the Head of the Electrical Engineering Department, City University of Science and Information Technology, Peshawar. He is also the Secretary of the Institutions of Engineer, Pakistan, Peshawar Center. His research interests include heterogeneous cellular networks, cognitive radio networks, and sensor networks.

ZIAUL HAQ ABBAS received the M.Phil. degree in electronics from Quaid-e-Azam University, Pakistan, in 2001, and the Ph.D. degree from the Agder Mobility Laboratory, Department of Information and Communication Technology, University of Agder, Norway, in 2012. He joined the Ghulam Ishaq Khan (GIK) Institute of Engineering Sciences and Technology, Pakistan, as a Research Associate. In 2012, he was a Visiting Researcher with the Department of Electrical and Computer Engineering, University of Minnesota, USA. He is currently an Associate Professor with the Faculty of Electrical Engineering and a Co-Founding Member of the Telecommunications and Networking (TeleCoN) Research Lab, GIK Institute. His research interests include energy efficiency in hybrid mobile and wireless communication networks, 4G and beyond mobile systems, mesh and ad hoc networks, traffic engineering in wireless networks, performance evaluation of communication protocols and networks by analysis and simulation, quality-of-service in wireless networks, green wireless communication, and cognitive radio.

GHULAM ABBAS (Senior Member, IEEE) received the B.S. degree in computer science from the University of Peshawar, Pakistan, in 2003, and the M.S. degree in distributed systems and the Ph.D. degree in computer networks from the University of Liverpool, U.K., in 2005 and 2010, respectively. From 2006 to 2010, he was Research Associate with Liverpool Hope University, U.K., where he was associated with the Intelligent and Distributed Systems Laboratory. Since 2011, he has been with the Faculty of Computer Sciences and Engineering, GIK Institute of Engineering Sciences and Technology, Pakistan. He is currently working as an Associate Professor and the Director of the Huawei Authorized Information and Network Academy. His research interests include computer networks, and wireless and mobile communications. He is also a Co-Founding Member of the Telecommunications and Networking (TeleCoN) Research Lab, GIK Institute. He is also a Fellow of the Institute of Science and Technology, U.K., and the British Computer Society.

NISAR AHMED received the B.S. degree in electrical and electronics engineering from the University College of Engineering and Technology Mirpur (A.K.), Pakistan, in 1989, and the Ph.D. degree in electrical and electronic engineering from the Imperial College of Science, Technology, and Medicine, London, U.K., in 1999. He is currently a Professor with the Faculty of Electrical Engineering, GIK Institute of Engineering Sciences and Technology, Pakistan. His current research interest includes transform techniques.

SUNGHWAN KIM received the B.S., M.S., and Ph.D. degrees from Seoul National University, South Korea, in 1999, 2001, and 2005, respectively. He was a Postdoctoral Visitor with the Georgia Institute of Technology (GeorgiaTech), from 2005 till 2007, and a Senior Engineer with Samsung Electronics, from 2007 till 2011. He is currently a Professor with the School of Electrical Engineering, University of Ulsan, South Korea. His main research interests are channel coding, modulation, massive MIMO, visible light communication, and quantum information.